Nuclear Inst. and Methods in Physics Research B 463 (2020) 16–20

Contents lists available at ScienceDirect

Nuclear Inst. and Methods in Physics Research B

journal homepage: www.elsevier.com/locate/nimb

A versatile time-of-flight medium-energy ion scattering setup using multiple delay-line detectors

Mauricio A. Sortica[a,c,*], Margareta K. Linnarsson[b], Dan Wessman[c], Svenja Lohmann[a], Daniel Primetzhofer[a,c]

[a] Department of Physics and Astronomy, Uppsala University, Box 516, SE-75120 Uppsala, Sweden
[b] Materials and Nano-Physics, KTH Royal Institute of Technology, Electrum 229, SE-16440 Kista, Sweden
[c] Tandem Laboratory, Uppsala University, Box 529, SE-75120 Uppsala, Sweden

ARTICLE INFO

Keywords:
Ion beam analysis
Time-of-flight
Medium-energy ion scattering
High resolution depth profiling

ABSTRACT

We present the most recent upgrades of the time-of-flight medium energy ion scattering (TOF-MEIS) system in Uppsala. The experimental chamber features a 6-axis goniometer with a sample annealing stage and two delay line detectors for composition analysis with high depth resolution and depth-resolved crystallography. The first detector has a large solid angle and can be moved circularly around the target position which allows to detect backscattered or transmitted ions. The second detector features increased flight distance from sample to detector resulting in enhanced energy resolution. A reduction from 1.4 keV to 0.4 keV is achieved for 100 keV He scattered from an Au surface for 1 ns time resolution, equivalent to a depth resolution of 6 Å. This detector is equipped with an electrostatic electrode in order to deflect charged particles, which allows to study the charge state for scattered ions in the medium energy regime.

1. Introduction

Medium-energy ion scattering (MEIS) is an ion beam analysis technique, developed for surface and near surface analysis [1,2] based on the same principles as Rutherford backscattering spectrometry (RBS) [3]. RBS has for several decades served as a powerful technique for quantitative composition depth profiling of solids from the energy spectrum of detected particles scattered from the sample. Although RBS typically employs light ions with a primary energy above 1 MeV, already in the 1960s–1970s experimental setups have been proposed, using medium-energy ions (typically 50–500 keV) and the channelling/blocking technique for a direct analysis of surface structures [4]. In this context, MEIS with a high resolution toroidal electrostatic analyzer (TEA) has been developed for simultaneous energy and scattering angle detection with a typical energy resolution $\Delta E/E = 4 \times 10^{-3}$ [1]. Despite its enhanced energy resolution, allowing subnanometric depth resolution, the TEA has the limitation of detecting ions exclusively, requiring knowledge on the charge state of the scattered particles for accurate depth profiling. Other setups based on time-of-flight have been proposed to overcome this limitation [5,6], but without reaching the same popularity as TEA. MEIS has been widely used not only for crystallography [7,8] but also for elemental depth profiling of ultra-thin films in electronic applications [9,10] and nanotechnology [11,12]. The renewed and broadened interest in the MEIS technique in the beginning of this century with increasing focus on single crystalline target materials, combined with much better technology for high-speed, position-sensitive detectors with improved lateral resolution, motivated the development of new time of flight MEIS systems (TOF-MEIS), usually employing a large area microchannel plates (MCP) detector [13–15].

A TOF-MEIS system with a delay-line anode detector has been installed at the Ångström Laboratory, Uppsala University in 2011, as reported in reference [14]. Since then, the system has been used in a series of applied research projects [16–18] and fundamental studies [19–22].

In this work we report a series of recent upgrades of the TOF-MEIS system in Uppsala. These new installations are: (i) an additional charge-discriminating delay line detector for simultaneous high resolution depth profiling and crystallography, (ii) a modified primary large angle detection system which allows the detection of electrons and features enhanced angular range permitting forward scattering geometries and transmission experiments, (iii) an electron bombardment heater unit for in-situ thermal annealing and (iv) an expansion of the load-lock chamber with a carrousel storage support for up to four samples. An overview of the unique capabilities of the system is presented together

* Corresponding author.
E-mail address: mauricio.sortica@physics.uu.se (M.A. Sortica).

https://doi.org/10.1016/j.nimb.2019.11.019
Received 24 June 2019; Received in revised form 13 September 2019; Accepted 11 November 2019
Available online 23 November 2019
0168-583X/

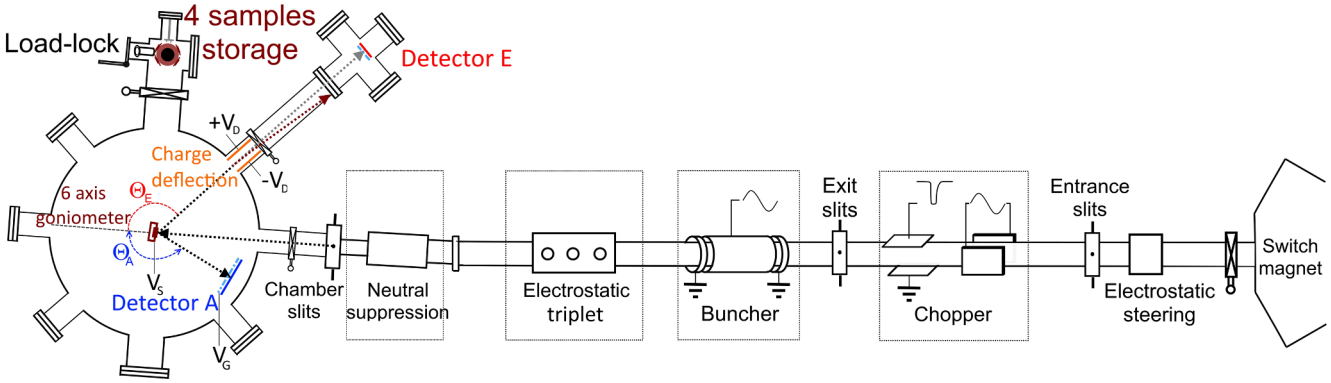

Fig. 1. Schematic illustration of the TOF-MEIS setup at Uppsala University, featuring a ~7 m long beam line with a chopper, a resonant tube buncher and an electrostatic quadrupole, as well as the experimental chamber with a 6-axis goniometer and 2 DLD detectors.

with some benchmarking experiments.

2. Experimental setup

2.1. Overview of the system

The TOF-MEIS setup, schematically illustrated in Fig. 1, consists of a beam line with a chopper system and an ultra-high vacuum experimental chamber, connected to a 350 kV air insulated accelerator from Danfysik. The three different operational modes of the ion source (sputter, gas and oven) allow for production of a wide range of positive primary ions, and masses in the range from 1 to 51 atomic mass units have already been successfully transmitted as beams to the MEIS-setup. Ion beams produced by the accelerator are typically chopped into short pulses by an electrostatic chopper using a horizontal 4 MHz sinusoidal scanning combined with a vertical gating pulse with adjustable frequency from 31.25 kHz to 1 MHz. An electrostatic triplet situated between chopper and the experimental chamber is used to obtain a focused beam at the sample. Sets of slits before and after the chopper, combined with an electrostatic steering at the beginning of the beam line, are used to get a narrow parallel pulsed beam, and a time resolution down to 1 ns can be achieved. A drift resonant-tube buncher can be used to compress the ion pulses in time thus enhancing the time resolution down to 0.3 ns [14]. This setup is optimized for 100 keV protons. Other combinations of ions and energies can be bunched, as long as the transit time of the pulse through the buncher $t_B = T(n + 1/2)$, where n is a non-negative integer and $T = 250$ ns is the period of the buncher voltage. Note, however, that within a certain band of about 20% around the optimum energy a significant net-compression of the beam packets in time can be achieved. A second electrostatic steering unit combined with a 7° bend of the beam line before the experimental chamber is used for suppression of neutral particles. A final collimation of the beam as well as position limiting is possible with another set of 4 independent slits positioned directly in front of the chamber. The time-of-flight of detected particles is measured from the chopper gating electrode to the detector. The beamline is kept at a pressure of $\sim 3 \times 10^{-6}$ mbar with two turbo pumps, one located before the chopper and the other before the neutral suppression.

The experimental chamber has an internal diameter of 70 cm and features a 6-axis goniometer equipped with a tungsten filament for the heating unit, a movable delay line detector DLD120 (*Detector A*) and an additional delay line detector DLD40 for enhanced energy resolution (*Detector E*). Assuming that the beam hits the surface of the sample at the center of the experimental chamber, the distance from the sample to the center of *Detector A* is 28.5 cm and to the center of *Detector E* is 105.0 cm. An electrostatic deflection electrode installed before *Detector E* allows for the detection of neutral scattered particles exclusively.

2.2. Time-of-flight detectors

Each detector is an MCP delay line detector from Roentdek, composed of a stack of circular microchannel plates mounted in chevron configuration on top of a delay line anode. The delay line anode is a copper plate (*holder*) framed at the four edges by ceramic insulators wrapped by two layers of helical wires, one for each spatial direction. Each layer is composed by a differential wire pair formed by a *signal* wire for data collection and a parallel *reference* wire kept at a potential difference of ~−36 V from *signal* [23]. The detector is usually biased for detection of positive particles by keeping the back contact of the MCPs at 0 V and applying −2.4 kV at the front MCP contact, 150 V at the *holder* and 250 V at the *signal* wires. The detectors can also be biased for detection of negative particles, e.g. electrons, by applying 2.7 kV on the MCP back contact and re-scaling all the other voltages accordingly [24]. A nickel grid is mounted at a distance of 1.8 cm in front of the MCP, in order to limit the extension of the electric field into the chamber volume. Voltages V_G between −500 V and 500 V can be applied.

The position of a hit event on a given spatial coordinate on one detector is obtained from the time difference from the signal arrival at both ends of the corresponding delay line. The time-of-flight of a hit is measured from the chopper gating signal to the MCP, with a flight distance corresponding to the distance from the exit slits to the target ($l_1 = 7$ m) plus the distance from the target to the detector (l_2).

Detector A has an active diameter of 120 mm and is mounted on a circular path around the center of the chamber, in which it can be moved in the horizontal plane, covering an interval of scattering angles from 0 to 160°, measured at its center. The distance $l_{2,A}$ is 285 mm measured at the detector center and since the surface of the detector is flat, increases radially for other positions. This geometry corresponds to an angular diameter of 24° covering a solid angle of 0.13 sr, allowing for direct measurements of blocking pattern of crystalline structures. Since the energy is obtained from the time of flight, the energy resolution will improve for longer flight times, i.e., for lower beam energy and heavier projectiles. Fig. 2 shows the energy resolution per energy of detected particles for H, He and Ne. Protons detected with 100 keV will yield an energy resolution of about 3.1 keV for 1 ns time resolution while helium atoms detected with the same energy will result in a resolution of 1.6 keV, and neon 0.7 keV (blue curves). For a bunched 100 keV proton beam, with a time resolution of 0.3 ns (blue dotted line of Fig. 2), a resolution of 0.9 keV is achieved.

Detector E has been added to the original setup described in [14] with a flight distance $l_{2,E} = 1050$ mm to increase the time-of-flight of the detected particles, resulting in enhanced energy resolution. It has a diameter of 40 mm and it is positioned at a scattering angle of 135°, covering a solid angle of 2 msr. For the example given above of particles detected with 100 keV, this corresponds to an improvement from

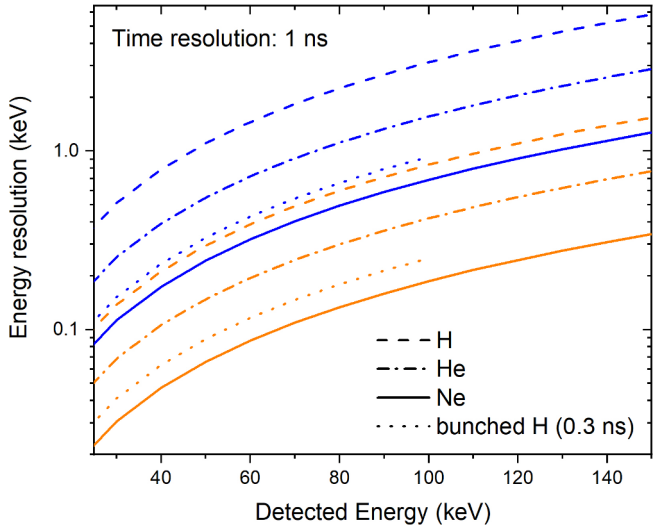

Fig. 2. Energy resolution as a function of the detected energy, converted from time-of-flight, for H, He and Ne, on *Detector A* (blue) and *Detector E* (orange) for a time resolution of 1 ns. The dotted lines highlight the energy resolution for 100 keV H beam using the buncher, with time resolution of 0.3 ns. (For interpretation of the references to colour in this figure legend, the reader is referred to the web version of this article.)

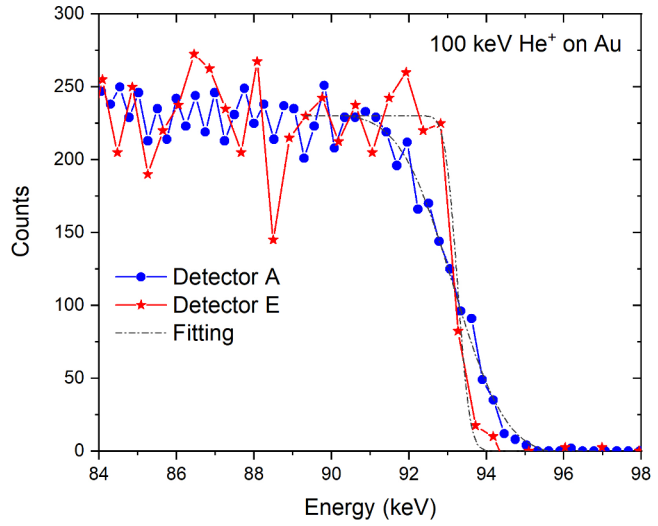

Fig. 3. Energy-converted ToF-MEIS spectrum for 100 keV He beam on gold, recorded simultaneously in both detectors A and E. The measured energy resolution for A and E is 2.96 keV and 0.74 keV, respectively, for a time resolution of 1.8 ns.

3.1 keV to 0.8 keV for protons and from 1.6 keV to 0.4 keV for helium, as shown by the orange curves of Fig. 2. This value, in turn, corresponds to a depth resolution of 0.6 nm in a gold target. Fig. 3 shows the MEIS spectrum for a 100 keV helium beam scattered from a polycrystalline gold sample, recorded simultaneously at both detectors with the incident beam aligned with the sample surface normal. A circular region at the center of *Detector A* corresponding to the solid angle of *Detector E* was selected for plotting the energy spectrum for comparison. The time resolution measured from the width of the photon peak in the TOF spectrum is 1.8 ns and the energy resolution measured from the slope of the gold front edge is 2.96 keV on *Detector A* and 0.74 keV on *Detector E*.

2.3. Charge deflection unit

An electrostatic deflection unit, consisting of 2 parallel metal plates

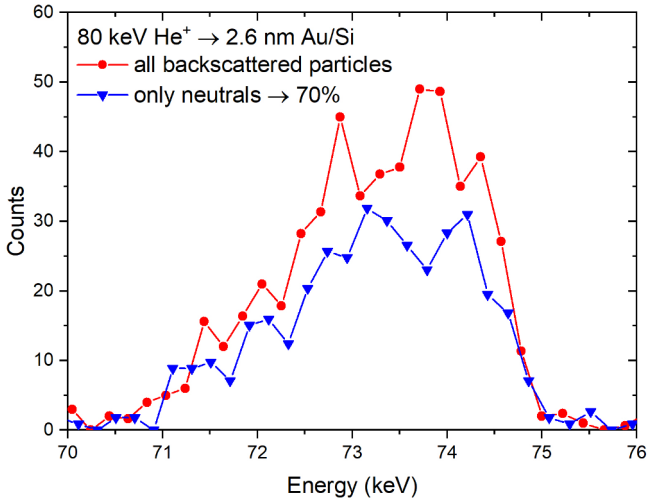

Fig. 4. Energy converted MEIS spectrum measured on *Detector E* for a 80 keV He beam on a thin gold film with 2.6 nm nominal thickness, with and without deflection of charged particles (red circles and blue triangles, respectively). (For interpretation of the references to colour in this figure legend, the reader is referred to the web version of this article.)

encased by a cylindrical metallic collimator has been installed between the goniometer and *Detector E*. This upgrade allows the investigation of charge exchange processes which are highly relevant for quantitative analysis using medium and low-energy ions [25,26]. A voltage ± V_D from 0 to 5 kV can be applied to the plates, as illustrated in Fig. 1, to deflect charged particles and to allow recording the spectrum of neutral particles exclusively. Fig. 4 shows spectra for 80 keV He scattered from a 2.6 nm thick polycrystalline gold film. By comparing the spectrum with and without deflection, the fraction of charged particles can be obtained, making it possible to investigate ion-charge states in matter for different projectiles and energies.

2.4. Sample annealing

The goniometer of the MEIS system has been equipped with an electron bombardment heater system for in-situ thermal annealing. The heating unit consists of an helicoidal tungsten filament with 0.15 mm diameter and a molybdenum anode. It has been installed on the goniometer, located behind the sample, and is connected to a VG Scienta UI42894K electron bombardment heater controller (EBHC) via one feedthrough at the chamber. Two of the three contacts for the pins of the sample holder are connected to a feedthrough for temperature monitoring via a thermocouple in contact with the sample. The sample can be heated by direct radiation from the filament or by electron bombardment, from room temperature up to 600 °C.

2.5. Load-lock chamber

The load-lock chamber can store up to 4 samples in high vacuum, $\sim 1 \times 10^{-7}$ mbar, which allows sequential measurements in the experimental chamber with high sample throughput. Samples can be transported in vacuum between the MEIS system and a new chamber for in-situ growth, modification and analysis of films built at the 5 MV 15SDH-2 Pelletron accelerator of the Tandem Laboratory at Uppsala University [27]. This transport is accomplished with a movable storage chamber with a turbo pump powered by batteries. This chamber is mounted on a wheel cart and can be lifted through a built-in jack to level up with the load-lock at MEIS. This allows in-situ growth characterization of films with both medium-energy and MeV-energy ion beam analysis.

3. Increased functionality of the present system

3.1. High-Resolution depth profiling with enhanced resolution

The increased energy resolution of *Detector E* allows depth profiling with a depth resolution of a few monolayers only. The best time resolution achievable with the use of the buncher for 100 keV protons is 0.3 ns and corresponds to an energy resolution below 0.25 keV on *Detector E* (see Fig. 2). This value is competitive with the values routinely achieved by the more common electrostatic analyzers, which typically operate with $\Delta E/E_0 \sim 4 \times 10^{-3}$ [1]. The demonstrated limit in energy resolution for the latter is found to be lower [11] at higher effective count rates. For such detectors, the energy for the charged ions is measured in a position sensitive detector by their deflection on the toroidal electrostatic analyzer, which results in a constant $\Delta E/E_0$ (depending of the beam stability), but is restricted to a narrow energy window for a specific charge state per acquisition, requiring several acquisitions to build the full energy spectrum, and a long acquisition time. The present system, in turn, detects and records the time-of-flight for all scattered particles resulting in a quicker acquisition with a constant time resolution (defined by the beam alignment, collimation and chopping) and much lower ion-induced damage to the samples due to the use of pulsed beams. Absolute quantification due to detection of all charge states presents another clear advantage of the present system in particular in comparison to using a He beam in a TEA-based system. Additionally, heavier projectiles can be used without restriction from multiple detected charge-states [26].

3.2. In-situ analysis and sample modification by thermal annealing

Our system allows in-situ characterization of the sample after modifications by ion irradiation and/or thermal annealing on the experimental chamber. The system has been used to study the formation of compounds such as silicides, which can also exhibit crystalline order for different annealing conditions [28]. Also, thin film analysis following step-wise in-situ annealing of plasma exposed surface has been performed [29]. For in-situ sputtering or implantations, the direct, unchopped primary ion beam can be used to hit the sample at selected incidence angles. Ion implantation in channeling or random directions can be performed by identifying the crystalline orientations with MEIS, heating the sample at the desired temperature and implanting the intended ion species at specific orientation with the crystalline axis of the target. This makes it possible to study temperature and channeling effects on doping of semiconductors by ion implantation [30]. Note, that for all these studies MEIS experiments can be performed at elevated temperatures, as long as the pressure of the experimental chamber can be kept below 1×10^{-7} mbar, which is required for safe operation of the detectors. When actively heating during the measurement, *Detector A* will be highly affected by photons emitted by the filament, resulting in a high level of background on the spectrum. This effect is much less intense on *Detector E* due to the collimator of the deflector electrodes.

3.3. Transmission experiments

Since *Detector A* can be rotated in an interval from 0 to 160° around the center of the chamber, it is possible to measure ions transmitted through thin freestanding samples, allowing for example to study the interaction of ions with 2D-materials [31]. For transmission measurements, a 5 cm long metal support with circular holes near the bottom for holding such samples can be attached to a regular sample holder. Mounted this way to the goniometer, the samples are positioned below it during the experiment, which still permits 3 translations as well as isocentric rotations of the polar angle. Up to 3 samples can be loaded in one holder. An example of a spectrum recorded for transmission of 50 keV He ions through an Au-foil with a nominal thickness of 141 nm is shown in Fig. 4. More details are given in Section 3.5.

3.4. Mass spectrometry

For typical TOF-MEIS experiments, the sample holder and the grid in front of the detector are grounded to avoid charge up of the sample during ion irradiation and to suppress electrostatic field due to the MCP front bias. Both the sample holder (V_S) and the grid in front of *Detector A* (V_G) can be biased to establish an accelerating electrostatic field between the sample and the detector. By applying $V_G \sim 500$ V and $V_S \leq 0$ and positioning the surface of the sample parallel to the detector, species desorbing from the surface of the sample will be accelerated towards the detector and will show up in the TOF spectrum. Mass spectrometry can be performed for positive desorbed particles with mass to charge ratio up to 1100 u and sufficient mass resolution to separate isotopes [32]. Negative particles can also be detected when the detector is biased with positive voltage at the front MCP contact, as discussed in the next section.

3.5. Detection of electrons

By biasing *Detector A* for detection of negative particles as described in the experimental setup section with the front MCP set to a positive potential (typically from 200 V to 300 V), secondary electrons induced by the ion beam can be measured. Detection efficiency can be increased by applying an electrostatic field with $V_S < 0$ and $V_G > 0$. Note that photons and backscattered or transmitted ions will still be detected. Fig. 5 shows a TOF spectrum acquired in transmission geometry for 50 keV He through a 141 nm thick gold foil. Photons, secondary electrons and transmitted ions are separated in time and can be identified in the spectrum. Note, that angular distributions can be recorded separately for all contributions to the spectrum which enables a series of fundamental studies

4. Summary

We report a series of upgrades of the TOF-MEIS setup at Uppsala University, now holding 2 delay line detectors, a sample heater and a sample storage stage.

The main characteristics of the setup are:

- Low ion fluence leading to very low damage to the sample due to the use of a pulsed beam;

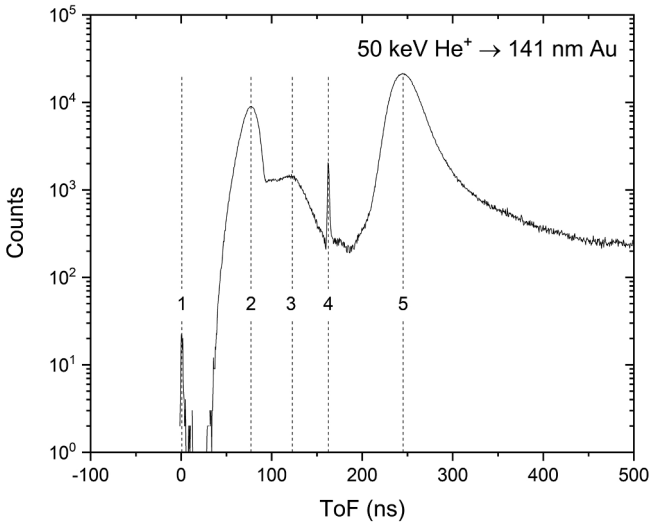

Fig. 5. Time-of-flight spectrum detected in transmission geometry using 50 keV He ions as projectiles and a free-standing 141 nm thick Au foil as a target. No voltages were applied to the sample and the grid. Signals corresponding to photons (1), secondary electrons (2 and 3), primary He ions transmitted through pinholes in the sample (4) and He ions transmitted through Au can be observed.

- *Detector A*, a movable large solid angle detector suitable for crystallography and short acquisition time usable in forward and backscattering geometries;
- *Detector E*, a detector with fixed scattering angle and long sample to detector distance suitable for high resolution depth profiling with sub-nanometric resolution;
- A charge deflection electrode before *Detector E* for study of the charge fractions of scattered particles;
- An electron bombardment heater for in-situ annealing, which can be combined with the MEIS for angle dependent hot implantation into crystalline targets;
- A load-lock chamber with storage for up to 4 samples and integration with the 5 MV Tandem accelerator;
- Sample holders for transmission experiments on free standing foils;
- Electrostatic acceleration from the sample to detector by the application voltage on the sample and the grid in front of the detector, for detection of desorbed particles and secondary electrons.

All the functionalities presented here can be combined to be operated simultaneously, except for sample heating. When the sample heating unit is used, it is not possible to apply a voltage V_S on the sample. In addition, heating is only available for backscattering experiments. Except for that, the detectors can operate together with the heating, restricted by the pressure on the experimental chamber and experimental noise caused by the filament.

The highly configurable character of our setup makes it a powerful experimental setup for many applications with a focus on in-situ studies, and it allows studying ion solid interactions in several dimensions and using coincidence measurements.

Acknowledgements

We would like to thank A. Czasch from Roentdek for the technical support on the installation and configuration of our detectors. We would also like to thank H. Winter (HU Berlin) for his valuable support. The operation of the TOF-MEIS system is supported by the Swedish Research Council VR-RFI, contracts #821-2012-5144 and #2017-00646_9, and the Swedish Foundation for Strategic Research (SSF) under contract RIF14-0053.

References

[1] R.G. Smeenk, R.M. Tromp, H.H. Kersten, A.J.H. Boerboom, F.W. Saris, Angle resolved detection of charged particles with a novel type toroidal electrostatic analyser, Nucl. Instruments Methods Phys. Res. 195 (1982) 581–586, https://doi.org/10.1016/0029-554X(82)90022-2.

[2] J.F. van der Veen, Ion beam crystallography of surfaces and interfaces, Surf. Sci. Rep. 5 (1985) 199–287, https://doi.org/10.1016/0167-5729(85)90001-9.

[3] W.-K. Chu, J.W. Mayer, M.-A. Nicolet, Backsterring Spectrometry, Academic Press, Orlando, 1978.

[4] W.C. Turkenburg, W. Soszka, F.W. Saris, H.H. Kersten, B.G. Colenbrander, Surface structure analysis by means of Rutherford scattering: methods to study surface relaxation, Nucl. Instruments Methods. 132 (1976) 587–602, https://doi.org/10.1016/0029-554X(76)90798-9.

[5] S.A. Agamy, J.E. Robinson, Surface analysis using medium energy ion and neutral scattering, Nucl. Instruments Methods. 149 (1978) 595–598, https://doi.org/10.1016/0029-554X(78)90934-5.

[6] M.H. Mendenhall, R.A. Weller, A time-of-flight spectrometer for medium energy ion scattering, Nucl. Instruments Methods Phys. Res. Sect. B Beam Interact. Mater. Atoms. 40–41 (1989) 1239–1243, https://doi.org/10.1016/0168-583X(89)90628-9.

[7] D.P. Woodruff, D. Brown, P.D. Quinn, T.C.Q. Noakes, P. Bailey, Structure determination of surface adsorption and surface alloy phases using medium energy ion scattering, Nucl. Instruments Methods Phys. Res. Sect. B Beam Interact. Mater. Atoms. 183 (2001) 128–139, https://doi.org/10.1016/S0168-583X(01)00472-4.

[8] J.C. Pillet, F. Pierre, D. Jalabert, Strain relaxation of CdTe on Ge studied by medium energy ion scattering, Nucl. Instruments Methods Phys. Res. Sect. B Beam Interact. Mater. Atoms. 384 (2016) 1–5, https://doi.org/10.1016/j.nimb.2016.07.020.

[9] E.P. Gusev, H.C. Lu, T. Gustafsson, E. Garfunkel, Growth mechanism of thin silicon oxide films on Si(100) studied by medium-energy ion scattering, Phys. Rev. B. 52 (1995) 1759–1775, https://doi.org/10.1103/PhysRevB.52.1759.

[10] J.M.J. Lopes, U. Littmark, M. Roeckerath, E. Durun Özben, S. Lenk, U. Breuer, A. Besmehn, A. Stärk, P.L. Grande, M.A. Sortica, C. Radtke, J. Schubert, S. Mantl, Isotopic labeling study of oxygen diffusion in amorphous LaScO3 high-κ films on Si (100) and its effects on the electrical characteristics, Appl. Phys. A Mater. Sci. Process. 96 (2009) 447–451, https://doi.org/10.1007/s00339-009-5153-y.

[11] H. Matsumoto, K. Mitsuhara, A. Visikovskiy, T. Akita, N. Toshima, Y. Kido, Au (core)/Pd(shell) structures analyzed by high-resolution medium energy ion scattering, Nucl. Instruments Methods Phys. Res. Sect. B Beam Interact. Mater. Atoms. 268 (2010) 2281–2284, https://doi.org/10.1016/j.nimb.2010.03.032.

[12] M.A. Sortica, P.L. Grande, G. MacHado, L. Miotti, Characterization of nanoparticles through medium-energy ion scattering, J. Appl. Phys. 106 (2009) 114320, , https://doi.org/10.1063/1.3266139.

[13] T. Kobayashi, Development of three-dimensional medium-energy ion scattering using a large solid angle detector, Nucl. Instruments Methods Phys. Res. Sect. B Beam Interact. Mater. Atoms. 249 (2006) 266–269, https://doi.org/10.1016/j.nimb.2006.04.066.

[14] M.K. Linnarsson, A. Hallén, J. Åström, D. Primetzhofer, S. Legendre, G. Possnert, New beam line for time-of-flight medium energy ion scattering with large area position sensitive detector, Rev. Sci. Instrum. 83 (2012) 095107, , https://doi.org/10.1063/1.4750195.

[15] K.W. Jung, H. Yu, W.J. Min, K.S. Yu, M.A. Sortica, P.L. Grande, D. Moon, Quantitative compositional profiling of conjugated quantum dots with single atomic layer depth resolution via time-of-flight medium-energy ion scattering spectroscopy, Anal. Chem. 86 (2014) 1091–1097, https://doi.org/10.1021/ac402753j.

[16] P. Ström, P. Petersson, R. Arredondo Parra, M. Oberkofler, T. Schwarz-Selinger, D. Primetzhofer, Sputtering of polished EUROFER97 steel: surface structure modification and enrichment with tungsten and tantalum, J. Nucl. Mater. 508 (2018) 139–146, https://doi.org/10.1016/J.JNUCMAT.2018.05.031.

[17] V. Paneta, S. Englund, S. Suvanam, J. Scragg, C. Platzer-Björkman, D. Primetzhofer, Ion-beam based characterization of TiN back contact interlayers for CZTS(e) thin film solar cells, Nucl. Instruments Methods Phys. Res. Sect. B Beam Interact. Mater. Atoms. (2018), https://doi.org/10.1016/j.nimb.2018.06.020.

[18] D. Primetzhofer, E. Dentoni Litta, A. Hallén, M.K. Linnarsson, G. Possnert, Ultra-thin film and interface analysis of high-k dielectric materials employing Time-Of-Flight Medium Energy Ion Scattering (TOF-MEIS), Nucl. Instruments Methods Phys. Res. Sect. B Beam Interact. Mater. Atoms. 332 (2014) 212–215, https://doi.org/10.1016/j.nimb.2014.02.063.

[19] D. Primetzhofer, Electronic stopping power of slow 20Ne ions in Au obtained from TOF-MEIS and Monte-Carlo computer simulations, Nucl. Instruments Methods Phys. Res. Sect. B Beam Interact. Mater. Atoms. 315 (2013) 26–29, https://doi.org/10.1016/J.NIMB.2013.05.063.

[20] M.K. Linnarsson, S. Khartsev, D. Primetzhofer, G. Possnert, A. Hallén, ToF-MEIS stopping measurements in thin SiC films, Nucl. Instruments Methods Phys. Res. Sect. B Beam Interact. Mater. Atoms. 332 (2014) 130–133, https://doi.org/10.1016/J.NIMB.2014.02.045.

[21] S. Lohmann, M.A. Sortica, V. Paneta, D. Primetzhofer, Analysis of photon emission induced by light and heavy ions in time-of-flight medium energy ion scattering, Nucl. Instruments Methods Phys. Res. Sect. B Beam Interact. Mater. Atoms. (2017), https://doi.org/10.1016/j.nimb.2017.08.005.

[22] M.A. Sortica, V. Paneta, B. Bruckner, S. Lohmann, T. Nyberg, P. Bauer, D. Primetzhofer, On the Z1-dependence of electronic stopping in TiN, Sci. Rep. 9 (2019) 176, https://doi.org/10.1038/s41598-018-36765-7.

[23] S.E. Sobottka, M.B. Williams, Delay line readout of microchannel plates, IEEE Trans. Nucl. Sci. 35 (1988) 348–351, https://doi.org/10.1109/23.12740.

[24] Roentdek, MCP delay line detector manual, (2019) 110. http://www.roentdek.com/manuals/MCPDelayLine manual.pdf.

[25] D. Primetzhofer, M. Spitz, S.N. Markin, E. Taglauer, P. Bauer, Influence of surface structure and composition on neutralization of 4He+ ions scattered from noble metals and alloy surfaces, Phys. Rev. B. 80 (2009) 125425, , https://doi.org/10.1103/PhysRevB.80.125425.

[26] Y. Kitsudo, K. Shibuya, T. Nishimura, Y. Hoshino, I. Vickridge, Y. Kido, Charge exchange of medium energy H and He ions emerging from solid surfaces, Nucl. Instruments Methods Phys. Res. Sect. B Beam Interact. Mater. Atoms. 267 (2009) 566–570, https://doi.org/10.1016/J.NIMB.2008.11.010.

[27] K.A. Kantre, M. V. Moro, D. Moldarev, D. Johansson, D. Wessman, M. Wolff, D. Primetzhofer, SIGMA: a Set-up for In-situ Growth, Material modification and Analysis by ion beams (this issue).

[28] T.T. Tran, L. Jablonka, B. Bruckner, S. Rund, D. Roth, M.A. Sortica, P. Bauer, Z. Zhang, D. Primetzhofer, Electronic interaction of slow hydrogen and helium ions with nickel-silicon systems, Phys. Rev. A 100 (2019) 032705, , https://doi.org/10.1103/PhysRevA.100.032705.

[29] P. Ström, D. Primetzhofer, T. Schwarz-Selinger, K. Sugiyama, Compositional and morphological analysis of FeW films modified by sputtering and heating, Nucl. Mater. Energy 12 (2017) 472–477, https://doi.org/10.1016/J.NME.2017.03.002.

[30] M.K. Linnarsson, A. Hallén, L. Vines, B.G. Svensson, Channeled implantations of p-Type dopants into 4H-SiC at different temperatures, Mater. Sci. Forum 963 (2019) 382–385, https://doi.org/10.4028/www.scientific.net/MSF.963.382.

[31] R. Wilhelm, E. Gruber, J. Schwestka, R. Heller, S. Fascko, F. Aumayr, R.A. Wilhelm, E. Gruber, J. Schwestka, R. Heller, S. Fascko, F. Aumayr, Neutralization dynamics of slow highly charged ions in 2D materials, Appl. Sci. 8 (2018) 1050, https://doi.org/10.3390/app8071050.

[32] S. Lohmann, D. Primetzhofer, Ion-induced particle desorption in time-of-flight medium energy ion scattering, Nucl. Instruments Methods Phys. Res. Sect. B Beam Interact. Mater. Atoms. 423 (2018) 22–26, https://doi.org/10.1016/j.nimb.2018.02.016.